

## **Supplementary Information**

# **Chemical Storage of Elemental Fluorine in Nanostructured Cerium Fluorides**

Valentine Camus-Génot,<sup>1</sup> Edouard Boivin,<sup>1</sup> Christophe Legein,<sup>1</sup> Monique Body,<sup>1</sup> Etienne Durand,<sup>2</sup> Alain Demourgues,<sup>2</sup> Marc Dubois,<sup>3</sup> Batiste Clavier,<sup>3</sup> Kévin Lemoine,<sup>3</sup> Vincent Sarou-Kanian,<sup>4</sup> Annie Hémon-Ribaud,<sup>1</sup> Vincent Maisonneuve,<sup>1</sup> Jérôme Lhoste,<sup>1\*</sup> Amandine Guiet<sup>1\*</sup>

<sup>1</sup> Institut des Molécules et Matériaux du Mans (IMMM), UMR 6283 CNRS, Le Mans Université, Avenue Olivier Messiaen, 72085 Le Mans Cedex 9, France

<sup>2</sup> Institut de Chimie de la Matière Condensée de Bordeaux (ICMCB), UMR 5026 CNRS, Université de Bordeaux, 33600 Pessac, France

<sup>3</sup> Institut de Chimie de Clermont Ferrand (ICCF), UMR 6002 CNRS, Université Clermont Auvergne, 63178 Aubière, France

<sup>4</sup> Conditions Extrêmes et Matériaux : Haute Température et Irradiation (CEMHTI), UPR 3079 CNRS, Université d'Orléans, 45071 Orléans, France

## **CORRESPONDING AUTHORS**

Amandine Guiet : [amandine.guiet@univ-lemans.fr](mailto:amandine.guiet@univ-lemans.fr)

Jérôme Lhoste: [jerome.lhoste@univ-lemans.fr](mailto:jerome.lhoste@univ-lemans.fr)

<b>Figure S1. Schematic representation of the different steps of OPIF synthesis methodology</b>	<b>4</b>
<b>Figure S2. Rietveld refinement of the powder X-ray diffraction patterns of CeF<sub>3</sub>-NP, CeF<sub>3</sub>-OPIF, CeO<sub>2</sub>-NP and CeO<sub>2</sub>-OPIF</b>	<b>4</b>
<b>Figure S3. Characterization of CeF<sub>3</sub> and CeO<sub>2</sub> NP by TEM, N<sub>2</sub> sorption and DLS</b>	<b>6</b>
<b>Figure S4. a) SEM image of dried PMMA particles. b) DLS analysis of PMMA particles in latex form. c) TGA analysis of dried PMMA beads under synthetic air</b>	<b>6</b>
<b>Figure S5. SEM, TEM, HRTEM and SAED patterns of a) macroporous CeF<sub>3</sub>-OPIF and b) CeO<sub>2</sub>-OPIF</b>	<b>7</b>
<b>Figure S6. a) Powder XRD patterns of pristine (NP) and macroporous (OPIF) materials. b) Nitrogen sorption isotherms of CeF<sub>3</sub>-OPIF and CeO<sub>2</sub>-OPIF</b>	<b>7</b>
<b>Figure S7. Schematic representation of F<sub>2</sub> fluorination line</b>	<b>8</b>
<b>Figure S8. a) Fluoride expansion assembly. b) Fluorination line under F<sub>2</sub>. c) Open half-shell furnace with reaction chamber</b>	<b>8</b>
<b>Figure S9. TEM images with corresponding SAED patterns of CeF<sub>3</sub>-NP, CeF<sub>3</sub>-OPIF, CeO<sub>2</sub>-NP and CeO<sub>2</sub>-OPIF after fluorination at different annealing temperatures from 250°C to 400°C under pure F<sub>2</sub> and for 3h</b>	<b>9</b>
<b>Figure S10. SEM images after fluorination under pure F<sub>2</sub> for 3h of CeF<sub>3</sub>-OPIF at a) 350°C and c) 400°C and CeO<sub>2</sub>-OPIF at b) 350°C and d) 400°C</b>	<b>10</b>
<b>Figure S11. Rietveld refinement of the powder X-ray diffraction patterns of CeF<sub>4</sub>, obtained by direct fluorination under pure F<sub>2</sub> flow for 3h at 350°C of a) CeF<sub>3</sub>-NP, b) CeO<sub>2</sub>-NP, c) CeF<sub>3</sub>-OPIF and d) CeO<sub>2</sub>-OPIF</b>	<b>11</b>
<b>Figure S12. <sup>19</sup>F solid state MAS experimental and fitted NMR spectra of CeF<sub>4</sub>·0.33H<sub>2</sub>O. The individual resonances used for the fit are shown below (see Table S4)</b>	<b>13</b>
<b>Figure S13. <sup>19</sup>F solid state MAS experimental and fitted NMR spectra of CeO<sub>2</sub>-OPIF-F<sub>2</sub>-350°C-day 1. The individual resonances used for the fit are shown below (see Table S5)</b>	<b>14</b>
<b>Figure S14. <sup>19</sup>F solid state MAS experimental and fitted NMR spectra of CeO<sub>2</sub>-OPIF-F<sub>2</sub>-350°C-day 7. The individual resonances used for the fit are shown below (see Table S6)</b>	<b>15</b>
<b>Figure S15. <sup>19</sup>F solid state MAS experimental and fitted NMR spectra of CeO<sub>2</sub>-OPIF-F<sub>2</sub>-350°C-day 38. The individual resonances used for the fit are shown below (see Table S7)</b>	<b>16</b>
<b>Figure S16. <sup>1</sup>H solid state MAS experimental and fitted NMR spectra of CeO<sub>2</sub>-OPIF fluorinated at 350°C, day 1, day 7 and day 38 and of CeF<sub>4</sub>·0.33H<sub>2</sub>O. The individual resonances used for the fit are shown below (see Table S8)</b>	<b>17</b>

<b>Figure S17. XRD patterns of CeF<sub>3</sub>-NP, CeF<sub>3</sub>-OPIF, CeO<sub>2</sub>-NP and CeO<sub>2</sub>-OPIF after defluorination under vacuum for 3h at different annealing temperatures</b>	<b>19</b>
<b>Figure S18. Rietveld refinement of the powder X-ray diffraction patterns of a) CeF<sub>3</sub>-NP-C1, b) CeO<sub>2</sub>-NP-C1, c) CeF<sub>3</sub>-OPIF-C1 and d) CeO<sub>2</sub>-OPIF-C1</b>	<b>19</b>
<b>Figure S19. Variable temperature PXRD study of CeF<sub>4</sub>·0.33H<sub>2</sub>O under N<sub>2</sub></b>	<b>20</b>
<b>Figure S20. Rietveld refinement of the powder X-ray diffraction patterns of commercial CeF<sub>4</sub>·0.33H<sub>2</sub>O a) as received and b) after one complete cycle (one defluorination and one fluorination)</b>	<b>21</b>
<b>Figure S21. PXRD study of fluorination(F)/defluorination(D) cycles of CeO<sub>2</sub>-OPIF</b>	<b>22</b>
<b>Figure S22. PXRD patterns recorded before (CeF<sub>4</sub>-2days / SiO<sub>2</sub>) and after (CeO<sub>2</sub>-OPIF-C1-2days / SiO<sub>2</sub> and CeO<sub>2</sub>-OPIF-C1-no break / SiO<sub>2</sub>) defluorination monitored by gas-phase infrared under nitrogen (N<sub>2</sub>) with the presence of SiO<sub>2</sub></b>	<b>22</b>

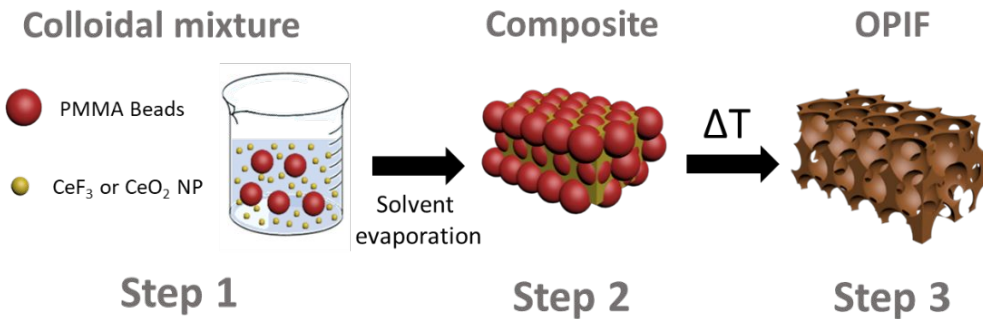


Figure S1. Schematic representation of the different steps of OPIF synthesis methodology.

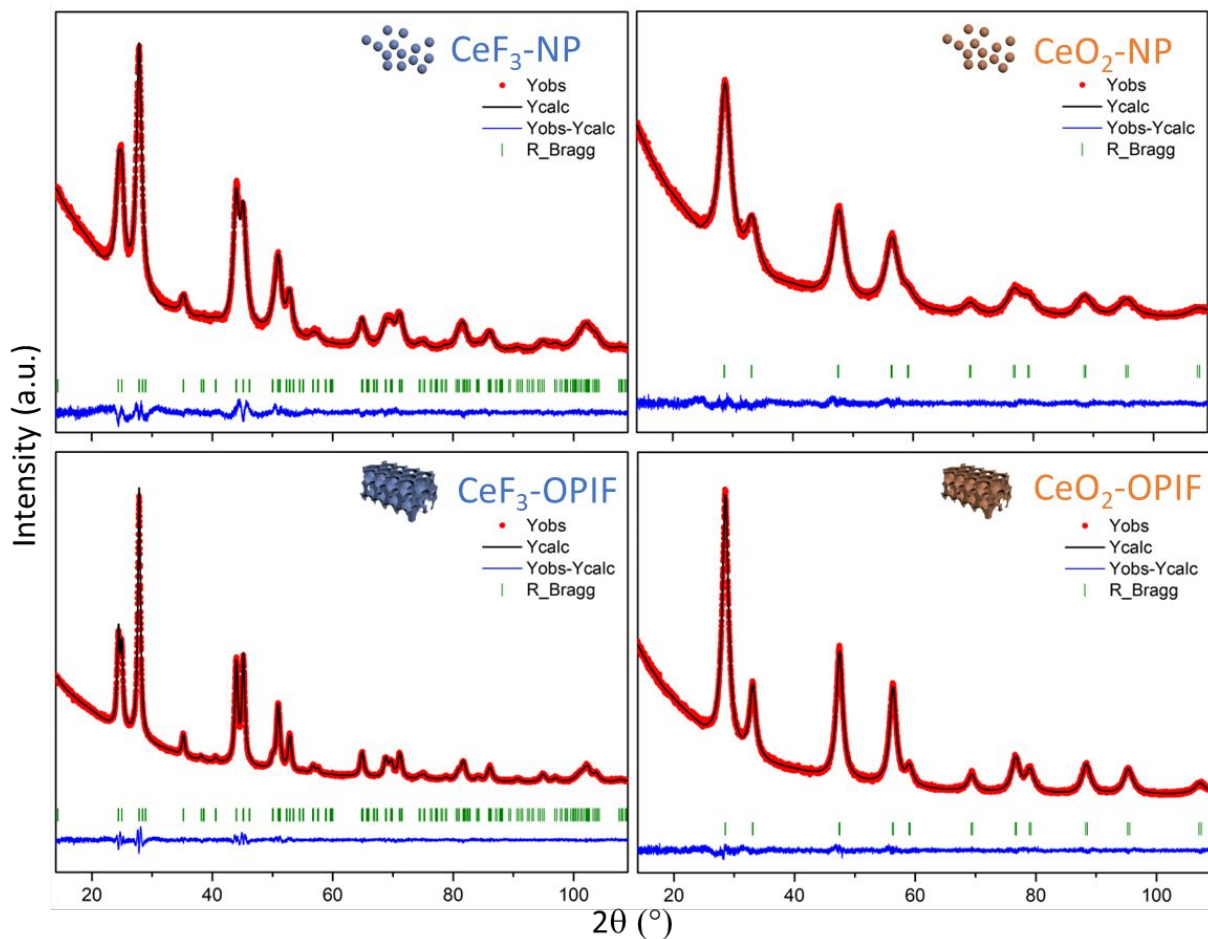


Figure S2. Rietveld refinement of the powder X-ray diffraction patterns of CeF<sub>3</sub>-NP, CeF<sub>3</sub>-OPIF, CeO<sub>2</sub>-NP and CeO<sub>2</sub>-OPIF. Experimental in red, calculated in black and difference in blue. Vertical green lines mark the positions of CeF<sub>3</sub> or CeO<sub>2</sub> reflections, depending on the considered material.

**Table S1.** Crystal data, data collection and structure refinement details of CeF<sub>3</sub>-NP, CeF<sub>3</sub>-OPIF, CeO<sub>2</sub>-NP and CeO<sub>2</sub>-OPIF. CeF<sub>3</sub> : Crystal system trigonal, space group: *P*<sup>3</sup>*c*1. CeO<sub>2</sub> : Crystal system cubic, space group: *Fm*<sup>3</sup>*m*. Radiation type: CuK<sub>α</sub>, 2θ range (°): 13-110.

Sample	CeF <sub>3</sub> NP	CeF <sub>3</sub> OPIF	CeO <sub>2</sub> NP	CeO <sub>2</sub> OPIF
Phase	CeF <sub>3</sub>	CeF <sub>3</sub>	CeO <sub>2</sub>	CeO <sub>2</sub>
a (Å)	7.1312(4)	7.1312(6)	5.4102(4)	5.41858(2)
c (Å)	7.2912(8)	7.2888(1)	-	-
V (Å <sup>3</sup> )	321.118(0)	321.011(6)	158.358(2)	159.095(7)
Number of reflections	239	191	19	19
Number of parameters	31	41	35	36
R <sub>p</sub> /R <sub>wp</sub> (%)	8.72/8.39	8.70/7.48	8.33/7.65	7.44/6.66
R <sub>B</sub> /R <sub>f</sub> (%)	1.20/0.91	1.02/1.12	0.56/0.32	0.53/0.31
χ <sup>2</sup>	2.44	2.06	1.49	1.48
Coherent domain size <L> (Å)	63.66	147.05	26.16	49.35

**Table S2.** Atomic positions and isotropic displacement parameters of CeF<sub>3</sub>-NP, CeF<sub>3</sub>-OPIF, CeO<sub>2</sub>-NP and CeO<sub>2</sub>-OPIF from powder X-ray Rietveld analysis.

Atom	Site	x	y	z	B <sub>iso</sub> (Å <sup>2</sup> )
<b>CeF<sub>3</sub>-NP</b>					
Ce1	6f	0.336(4)	0	1/4	0.505(8)
F1	12g	0.303(1)	0.022(1)	0.577(6)	1.164(1)
F2	4d	2/3	1/3	0.305(8)	0.344(1)
F3	2a	0	0	1/4	1.444(1)
<b>CeF<sub>3</sub>-OPIF</b>					
Ce1	6f	0.343(1)	0	1/4	0.530(0)
F1	12g	0.359(1)	0.050(2)	0.577(2)	1.714(1)
F2	4d	2/3	1/3	0.312(4)	0.838(1)
F3	2a	0	0	1/4	1.935(1)
<b>CeO<sub>2</sub>-NP</b>					
Ce1	4a	0	0	0	1.752(2)
O1	8c	1/4	1/4	1/4	1.406(7)
<b>CeO<sub>2</sub>-OPIF</b>					
Ce1	4a	0	0	0	1.945(7)
O1	8c	1/4	1/4	1/4	2.197(5)

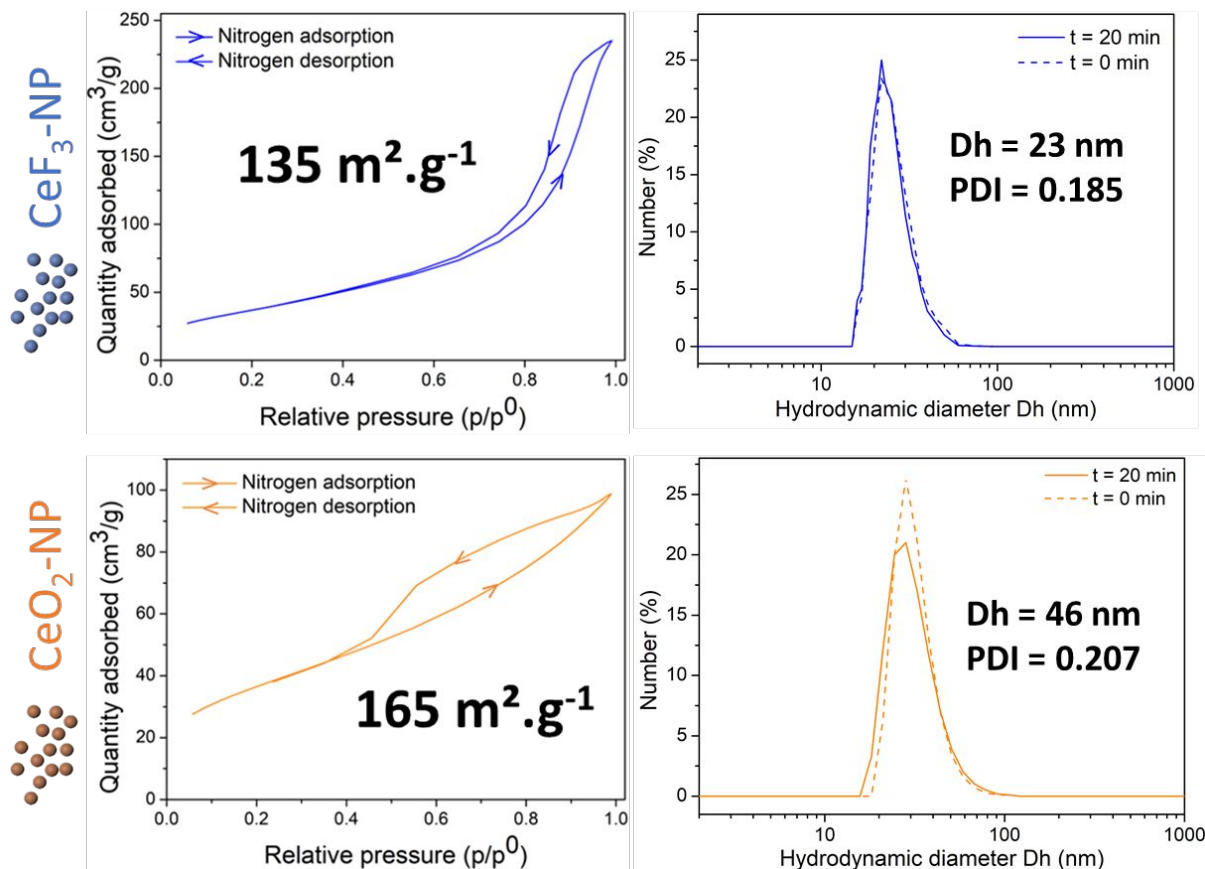


**Figure S3.** Characterization of CeF<sub>3</sub> (top) and CeO<sub>2</sub> (bottom) NP by TEM (left), N<sub>2</sub> sorption (middle) and DLS (right).

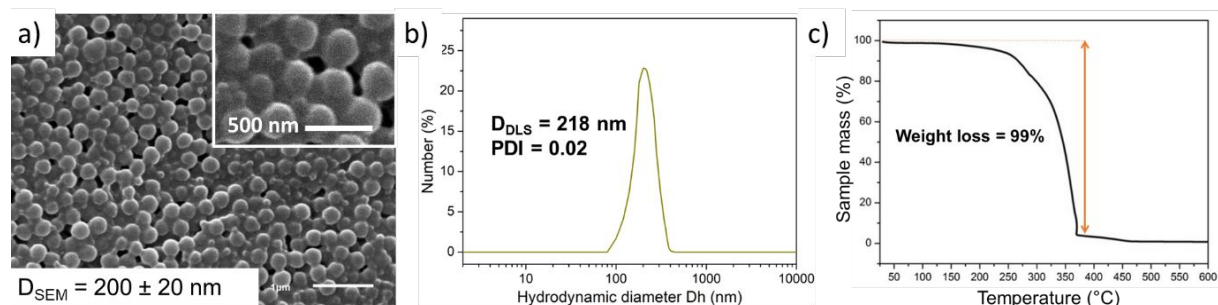


**Figure S4.** a) SEM image of dried PMMA particles. b) DLS analysis of PMMA particles in latex form. c) TGA analysis of dried PMMA beads under synthetic air.

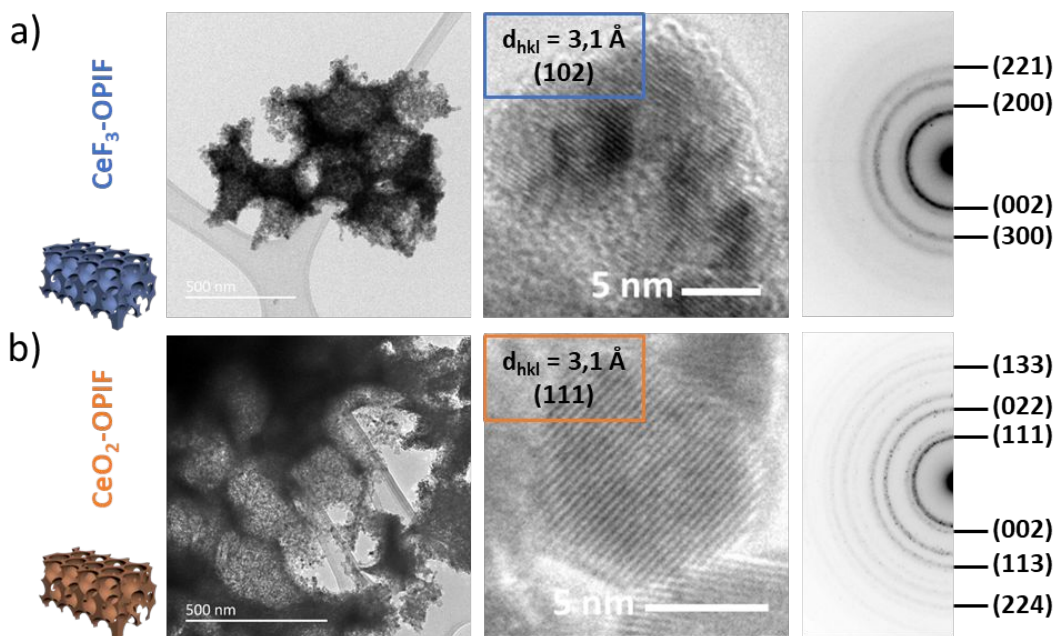


Figure S5. TEM, HRTEM and SAED patterns of a) macroporous  $\text{CeF}_3$ -OPIF and b)  $\text{CeO}_2$ -OPIF.

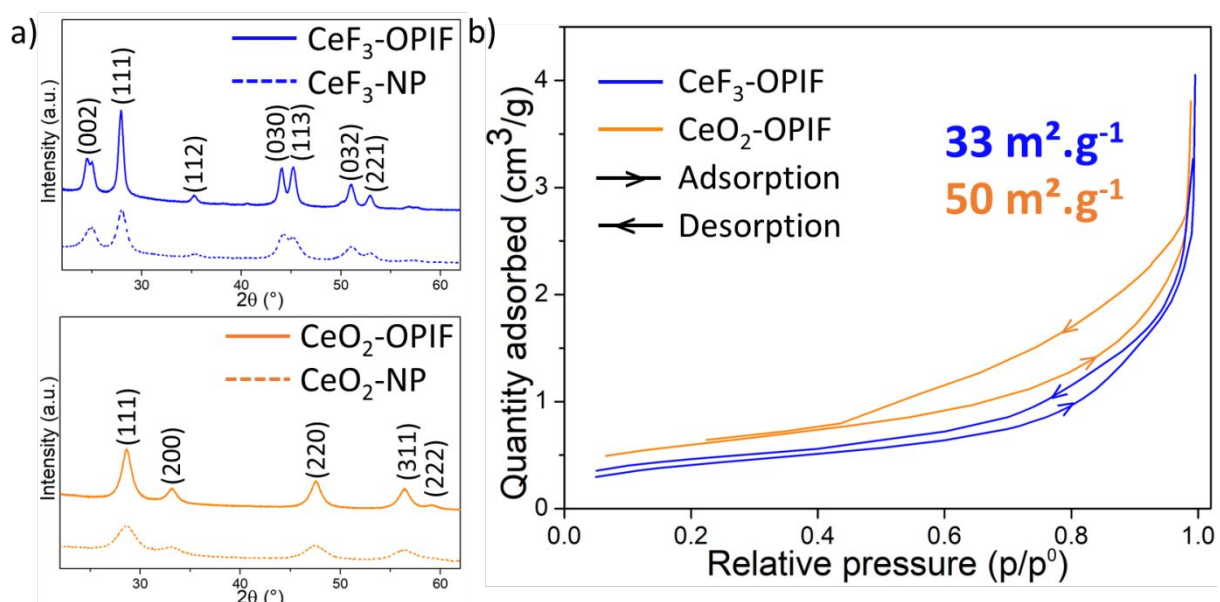


Figure S6. a) Powder XRD patterns of pristine (NP) and macroporous (OPIF) materials. b) Nitrogen sorption isotherms of  $\text{CeF}_3$ -OPIF and  $\text{CeO}_2$ -OPIF.

Table S3. Comparison of particle sizes and surface area of  $\text{CeF}_3$ -NP,  $\text{CeF}_3$ -OPIF,  $\text{CeO}_2$ -NP and  $\text{CeO}_2$ -OPIF determined by XRD ( $D_{\text{XRD}}$ ), TEM ( $D_{\text{TEM}}$ ) and  $N_2$  sorption ( $S_{\text{BET}}$ ).

Sample	$\text{CeF}_3$ -NP	$\text{CeF}_3$ -OPIF	$\text{CeO}_2$ -NP	$\text{CeO}_2$ -OPIF
$S_{\text{BET}}$ ( $\text{m}^2/\text{g}$ )	$135 \pm 5$	$33 \pm 5$	$165 \pm 5$	$50 \pm 5$
$D_{\text{TEM}}$ (nm)	$5 \pm 1$	$7 \pm 2$	$5 \pm 1$	$7 \pm 2$
$D_{\text{XRD}}$ (nm)	$8 \pm 1$	$10 \pm 1$	$3 \pm 1$	$7 \pm 1$

## F<sub>2</sub> fluororation line

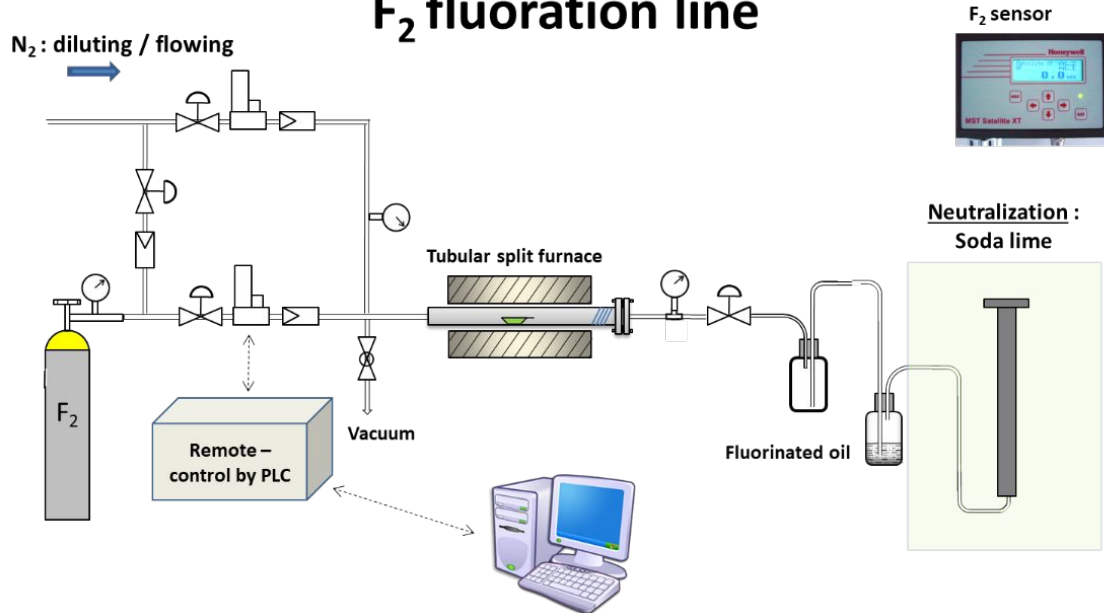


Figure S7. Schematic representation of F<sub>2</sub> fluorination line.

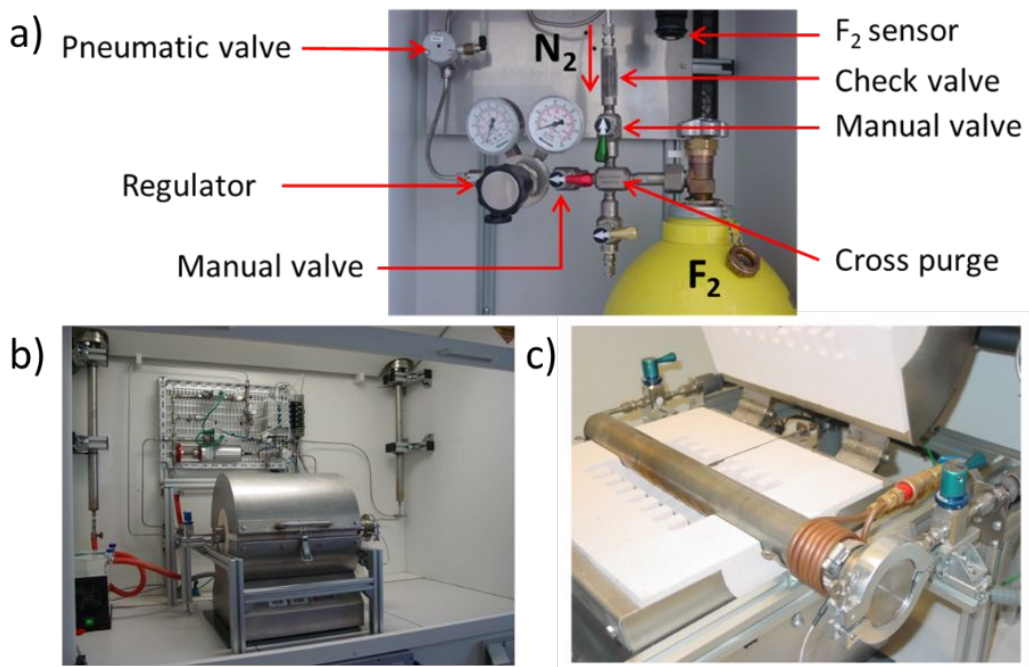
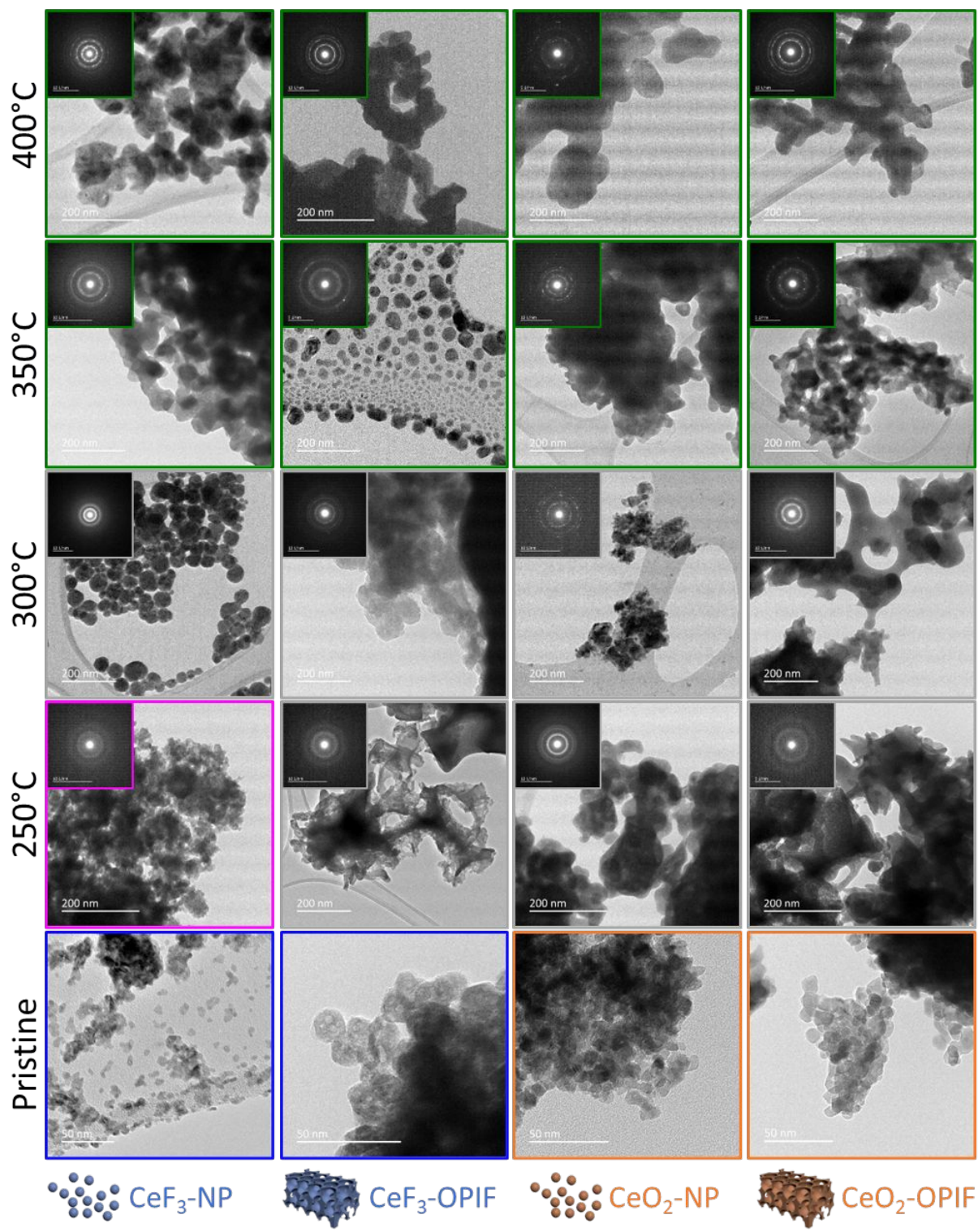
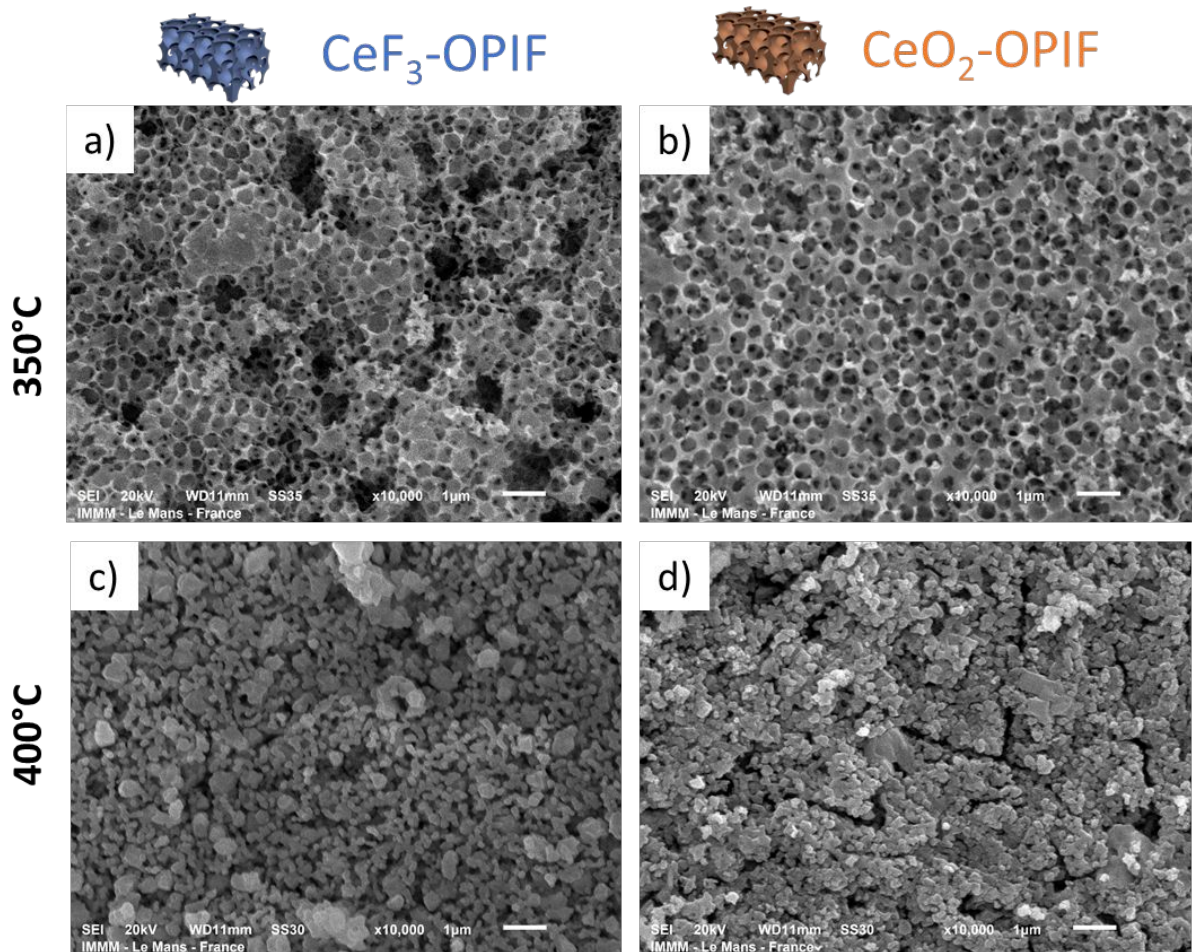


Figure S8. a) Fluoride expansion assembly. b) Fluorination line under F<sub>2</sub>. c) Open half-shell furnace with reaction chamber.



**Figure S9.** TEM images with corresponding SAED patterns of CeF<sub>3</sub>-NP, CeF<sub>3</sub>-OPIF, CeO<sub>2</sub>-NP and CeO<sub>2</sub>-OPIF after fluorination at different annealing temperatures from 250°C to 400°C under pure F<sub>2</sub> and for 3h.



**Figure S10.** SEM images after fluorination under pure F<sub>2</sub> for 3h of CeF<sub>3</sub>-OPIF at a) 350°C and c) 400°C and CeO<sub>2</sub>-OPIF at b) 350°C and d) 400°C.

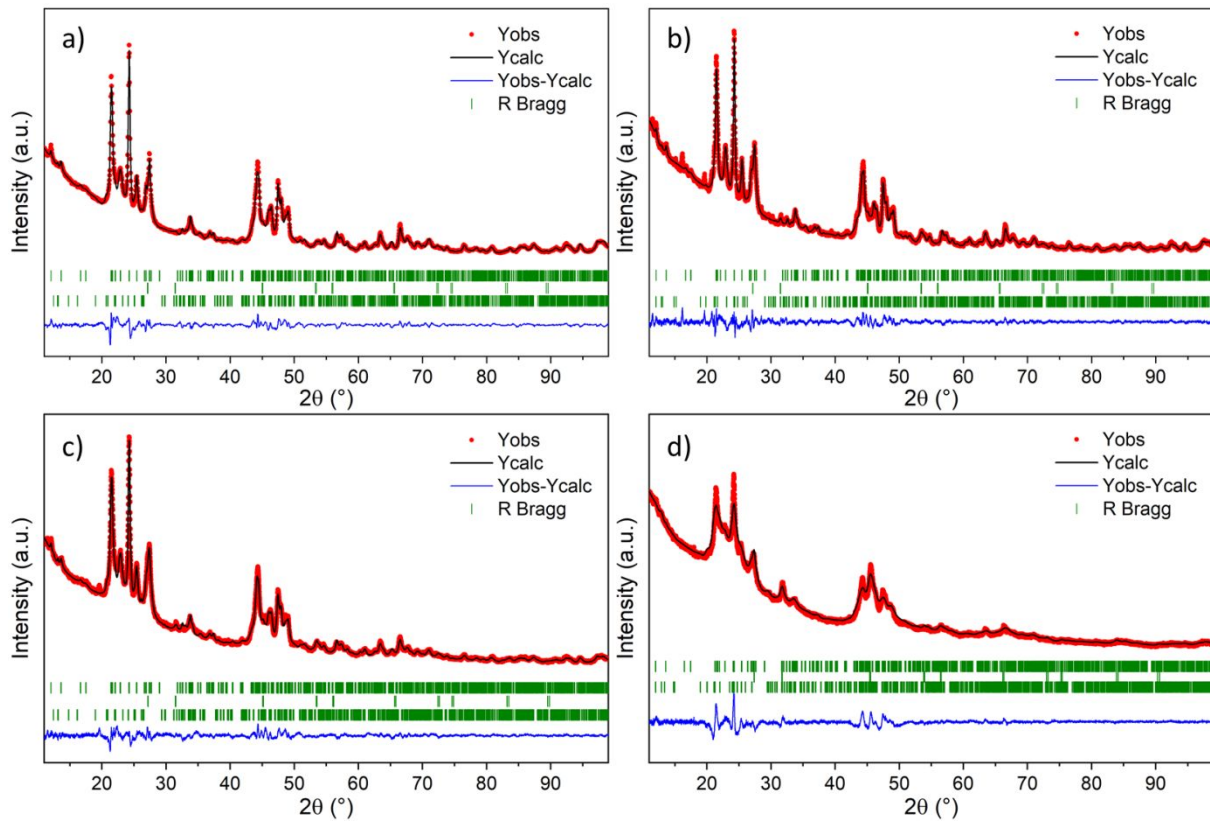


**Figure S11.** Rietveld refinement of the powder X-ray diffraction patterns of  $\text{CeF}_4$ , obtained by direct fluorination under pure  $\text{F}_2$  flow for 3h at  $350^\circ\text{C}$  of a)  $\text{CeF}_3$ -NP, b)  $\text{CeO}_2$ -NP, c)  $\text{CeF}_3$ -OPIF and d)  $\text{CeO}_2$ -OPIF. Experimental in red, calculated in black and difference in blue. Vertical green lines mark the positions of  $\text{CeF}_4$ ,  $\text{CeF}_4 \cdot 0.33\text{H}_2\text{O}$  and  $\text{CeOF}$  reflections.

**Table S4.** Crystal data, data collection and structure refinement details of  $\text{CeF}_3$ -NP,  $\text{CeF}_3$ -OPIF,  $\text{CeO}_2$ -NP and  $\text{CeO}_2$ -OPIF after fluorination at  $350^\circ\text{C}$  under pure  $\text{F}_2$  flow.  $\text{CeF}_4$ : crystal system monoclinic, space group:  $C2/c$ . Radiation type:  $\text{CuK}\alpha$ ,  $2\theta$  range ( $^\circ$ ): 13-110.

Sample	$\text{CeF}_3$ NP	$\text{CeF}_3$ OPIF	$\text{CeO}_2$ NP	$\text{CeO}_2$ OPIF
Phase after fluorination	$\text{CeF}_4$	$\text{CeF}_4$	$\text{CeF}_4$	$\text{CeF}_4$
a ( $\text{\AA}$ )	12.5924(6)	12.6022(6)	12.5839(5)	12.6059(4)
b ( $\text{\AA}$ )	10.6361(1)	10.6422(5)	10.6310(5)	10.7646(3)
c ( $\text{\AA}$ )	8.2363(0)	8.2379(9)	8.2354(1)	8.2303(9)
$\beta$ ( $^\circ$ )	126.3143(9)	126.3720(2)	126.2916(7)	126.2931(5)
$V$ ( $\text{\AA}^3$ )	888.88	889.61	888.02	900.18
Number of reflections	459	663	560	663
Number of parameters	88	75	99	91
$R_p/R_{wp}$ (%)	10.6/11.1	11.7/11.4	13.2/12.9	16.1/17.1
$R_B/R_f$ (%)	3.33/1.99	3.11/2.13	3.24/1.87	10.5/7.59
$\chi^2$	11.3	4.37	4.34	7.91
Coherent domain size $\langle L \rangle$ ( $\text{\AA}$ )	178	146	196	46

**Table S5. Composition of CeF<sub>3</sub>-NP and -OPIF and CeO<sub>2</sub>-NP and -OPIF after fluorination under 100% F<sub>2</sub> at 350°C for 3h and after one week of exposure to ambient air.**

Samples after F <sub>2</sub> -350°C	CeF <sub>3</sub> -NP	CeF <sub>3</sub> -OPIF	CeO <sub>2</sub> -NP	CeO <sub>2</sub> -OPIF
% mol CeF <sub>4</sub>	89	87	80	60
% mol CeOF	6	7	7	3
% mol CeF <sub>4</sub> ·0.33H <sub>2</sub> O	5	6	13	37
D <sub>XRD</sub> (nm)	24±2	12±1	26±2	6±1

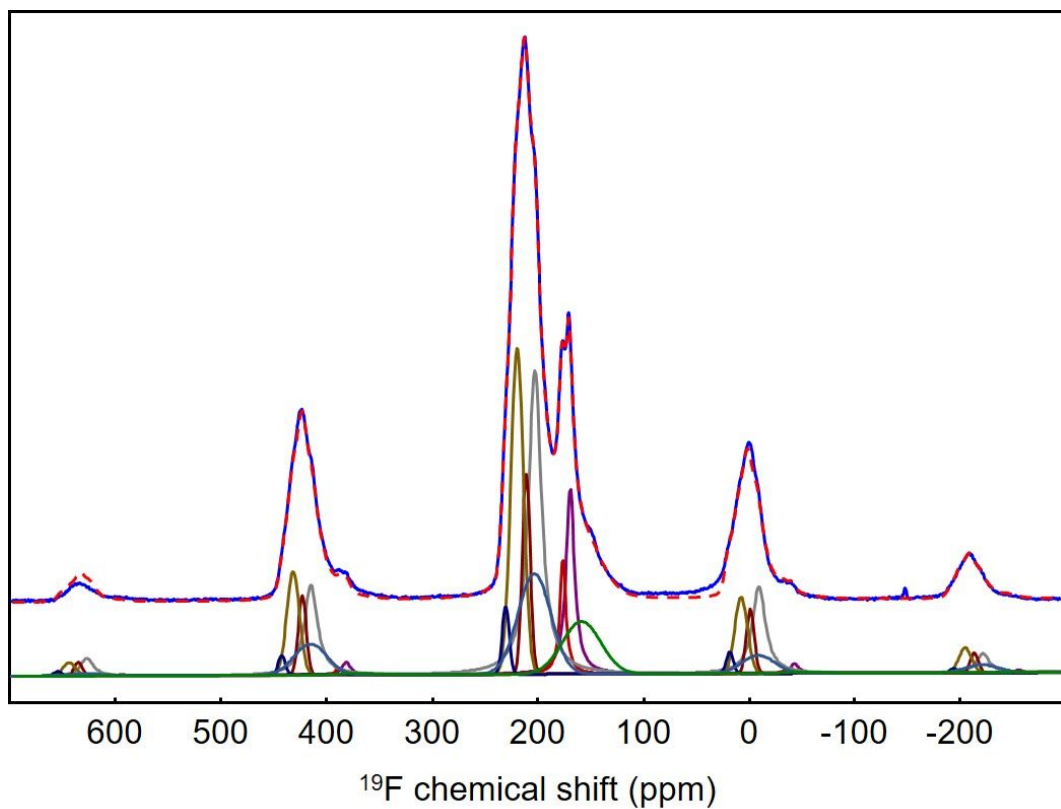


**Figure S12.**  $^{19}\text{F}$  solid state MAS (60 kHz) experimental (blue line) and fitted (dashed red line) NMR spectra of  $\text{CeF}_4 \cdot 0.33\text{H}_2\text{O}$ . The individual resonances used for the fit are shown below (see Table S4). The small resonance at -151 ppm is assigned to an unidentified impurity.

**Table S6.** Isotropic chemical shifts  $\delta_{\text{iso}}$  (ppm), line widths LW (ppm) and relative intensities I (%), of the NMR lines used for the fits of the  $^{19}\text{F}$  solid state MAS (60 kHz) NMR spectrum of  $\text{CeF}_4 \cdot 0.33\text{H}_2\text{O}$ .

$\delta_{\text{iso}}$	LW	I
157.9	43.1	6.6
169.4	9.5	8.2
176.4	6.8	3.6
202.9	14.9	32.0
203.3	36.5	16.4
211.0	8.8	9.3
219.7	14.0	21.4
230.5	7.7	2.5

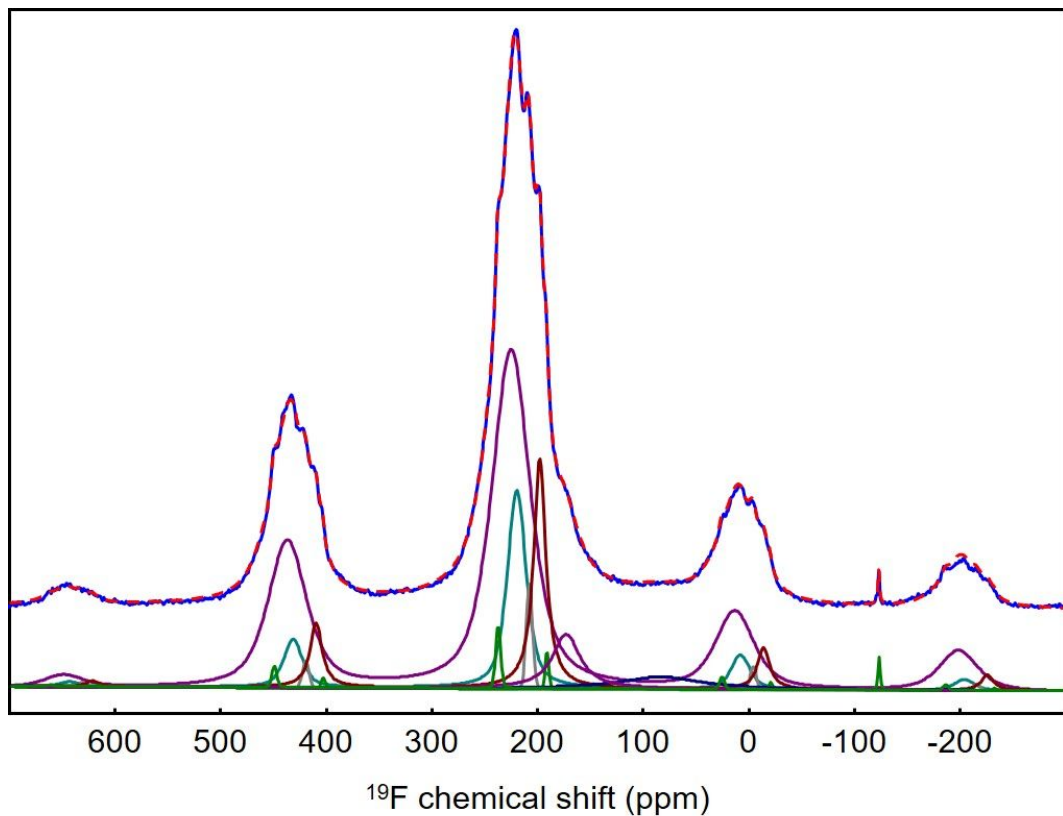


**Figure S13.**  $^{19}\text{F}$  solid state MAS (60 kHz) experimental (blue line) and fitted (dashed red line) NMR spectra of  $\text{CeO}_2\text{-OPIF-F}_2\text{-350}^\circ\text{C}$ -day 1. The individual resonances used for the fit are shown below (see Table S5). The small resonance at -123 ppm is assigned to an unidentified impurity.

**Table S7.** Isotropic chemical shifts  $\delta_{\text{iso}}$  (ppm), line widths LW (ppm) and relative intensities I (%) of the NMR lines used for the fits of the  $^{19}\text{F}$  solid state MAS (60 kHz) NMR spectrum of  $\text{CeO}_2\text{-OPIF-F}_2\text{-350}^\circ\text{C}$ -day 1 at  $350^\circ\text{C}$ , day 1.

$\delta_{\text{iso}}$	LW	I
83.6	92.3	2.9
173.3	31.5	4.5
191.4	3.9	0.4
198.2	13.8	13.1
208.1	7.0	2.1
220.0	21.1	14.4
225.4	43.4	61.4
237.5	5.6	1.1

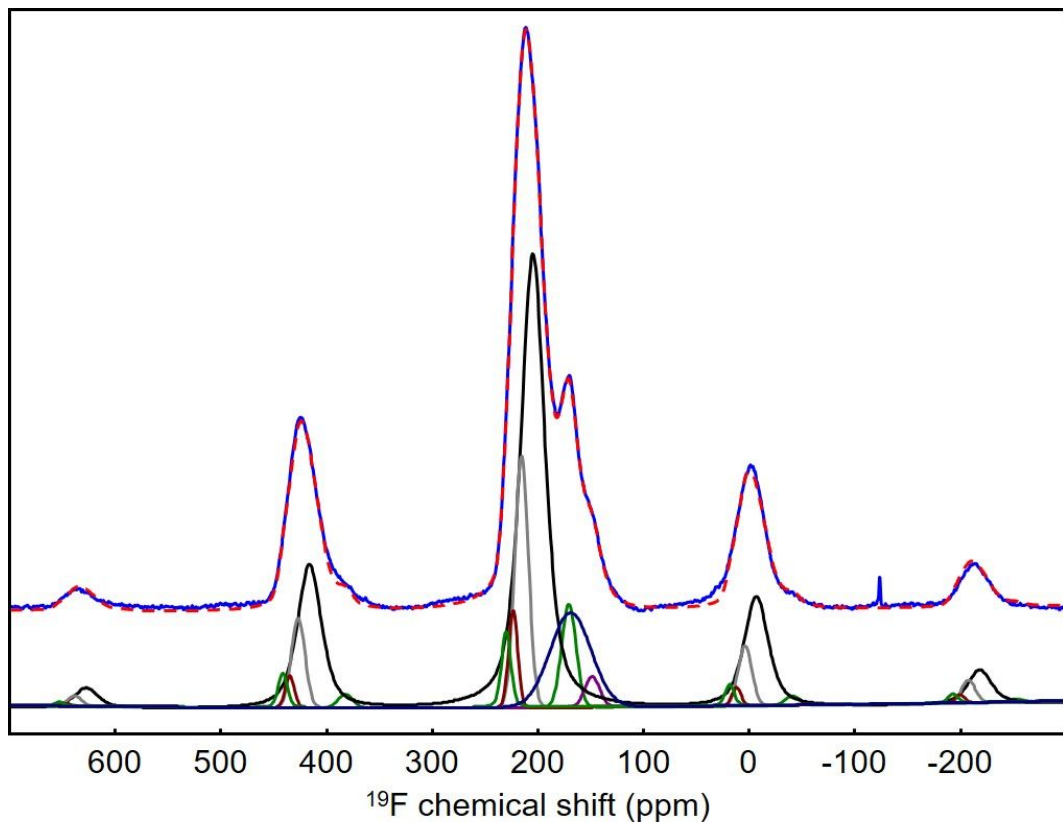


**Figure S14.**  $^{19}\text{F}$  solid state MAS (60 kHz) experimental (blue line) and fitted (dashed red line) NMR spectra of  $\text{CeO}_2\text{-OPIF-F}_2\text{-350}^\circ\text{C}$ -day 7. The individual resonances used for the fit are shown below (see Table S6). The small resonance at -123 ppm is assigned to an unidentified impurity.

**Table S8.** Isotropic chemical shifts  $\delta_{\text{iso}}$  (ppm), line widths LW (ppm) and relative intensities I (%) of the NMR lines used for the fits of the  $^{19}\text{F}$  solid state MAS (60 kHz) NMR spectrum of  $\text{CeO}_2\text{-OPIF-F}_2\text{-350}^\circ\text{C}$ -day 7.

$\delta_{\text{iso}}$	LW	I
148.6	16.5	1.2
169.0	45.4	10.0
170.6	16.2	4.9
204.7	27.0	60.9
215.4	15.1	15.3
223.4	10.1	3.7
230.0	10.3	3.9

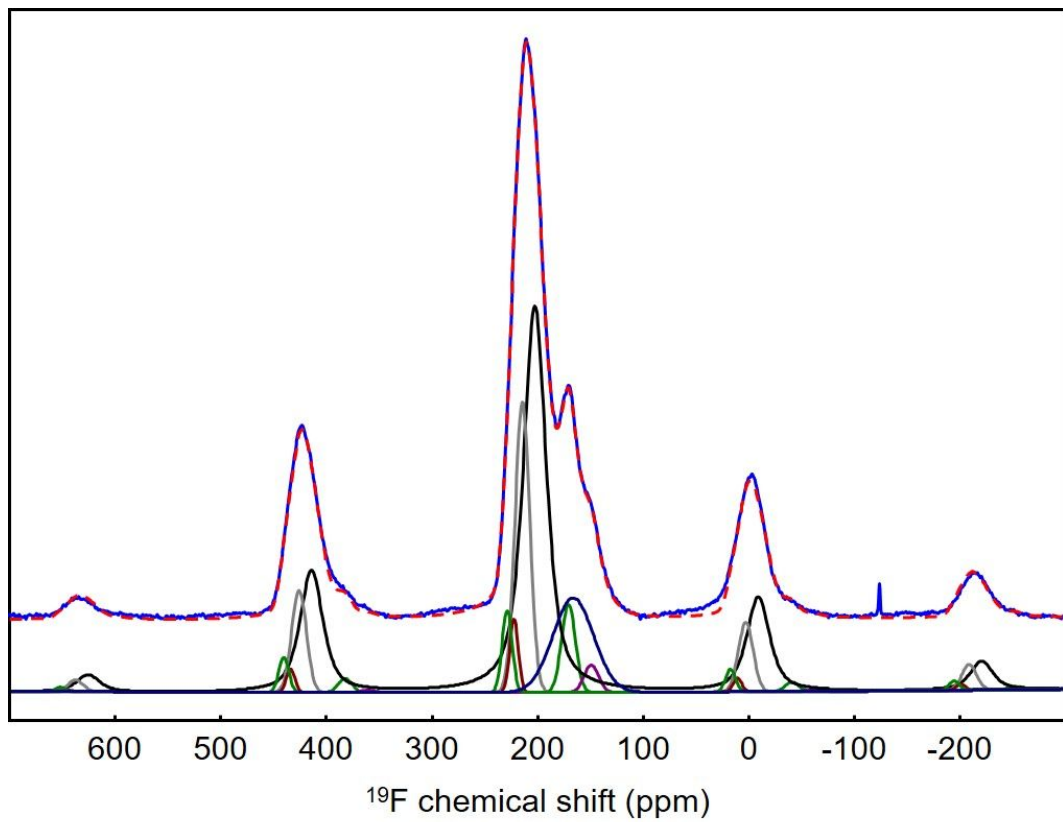


**Figure S15.**  $^{19}\text{F}$  solid state MAS (60 kHz) experimental (blue line) and fitted (dashed red line) NMR spectra of  $\text{CeO}_2\text{-OPIF-F}_2\text{-350}^\circ\text{C-day 38}$ . The individual resonances used for the fit are shown below (see Table S7). The small resonance at -123 ppm is assigned to an unidentified impurity.

**Table S9.** Isotropic chemical shifts  $\delta_{\text{iso}}$  (ppm), line widths LW (ppm) and relative intensities I (%) of the NMR lines used for the fits of the  $^{19}\text{F}$  solid state MAS (60 kHz) NMR spectrum of  $\text{CeO}_2\text{-OPIF-F}_2\text{-350}^\circ\text{C-day 38}$ .

$\delta_{\text{iso}}$	LW	I
149.4	16.0	1.3
166.5	45.1	10.8
171.1	15.3	4.5
202.9	25.7	55.3
214.7	16.3	20.8
222.6	9.5	2.9
229.1	11.0	4.4

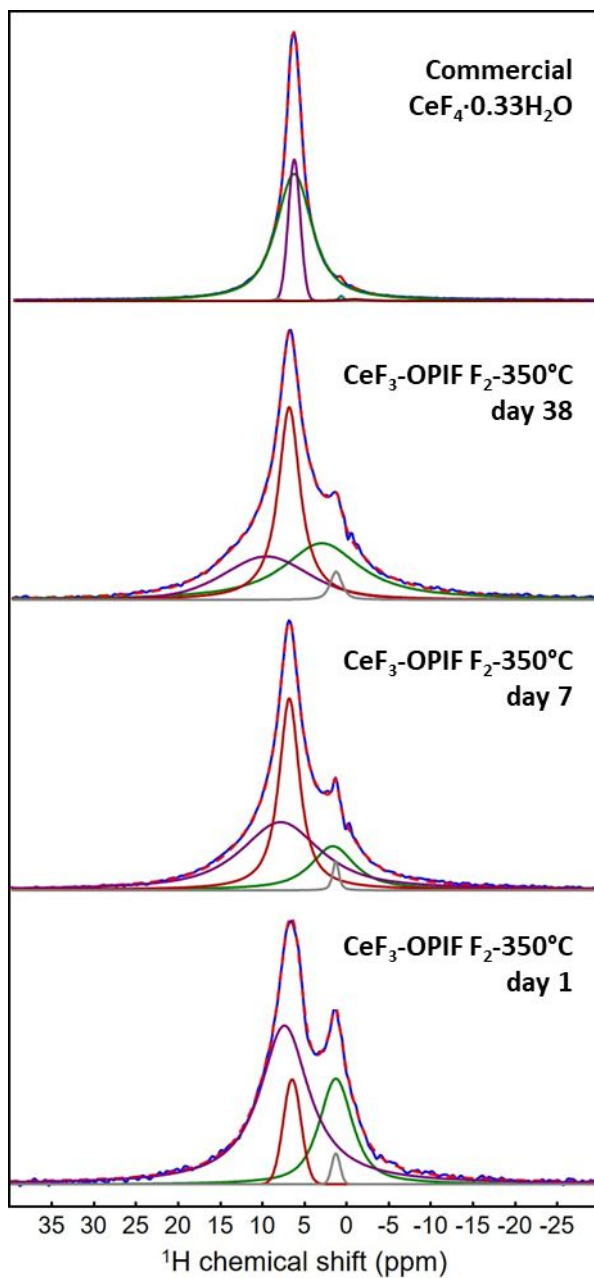


**Figure S16.**  $^1\text{H}$  solid state MAS (60 kHz) experimental (blue line) and fitted (dashed red line) NMR spectra of  $\text{CeO}_2$ -OPIF fluorinated at  $350^\circ\text{C}$ , day 1, day 7 and day 38 and of  $\text{CeF}_4 \cdot 0.33\text{H}_2\text{O}$ . The individual resonances used for the fit are shown below (see Table S8).

**Table S10.** Isotropic chemical shifts  $\delta_{\text{iso}}$  (ppm), line widths LW (ppm), relative intensities I (%) and assignment of the NMR lines used for the fits of the  $^1\text{H}$  solid state MAS (60 kHz) NMR spectra of  $\text{CeO}_2$ -OPIF-F<sub>2</sub>-350°C-day 1, day 7 and day 38 and of commercial  $\text{CeF}_4 \cdot 0.33\text{H}_2\text{O}$ .

Sample	$\delta_{\text{iso}}$	LW	I	Assignment
$\text{CeO}_2$ -OPIF-F <sub>2</sub> -350°C, day 1	1.3	4.7	25.6	OH
	1.3	1.2	1.5	OH
	6.5	2.5	10.5	OH & H <sub>2</sub> O
	7.4	7.0	62.5	OH & H <sub>2</sub> O
$\text{CeO}_2$ -OPIF-F <sub>2</sub> -350°C, day 7	1.5	0.9	1.5	OH
	1.8	6.1	16.9	OH
	7.0	2.9	36.6	OH & H <sub>2</sub> O
	8.0	11.2	45.0	OH & H <sub>2</sub> O
$\text{CeO}_2$ -OPIF-F <sub>2</sub> -350°C, day 38	1.5	1.7	2.6	OH
	3.2	11.0	34.9	OH
	7.1	3.1	37.1	OH & H <sub>2</sub> O
	9.8	12.0	25.4	OH & H <sub>2</sub> O
Commercial $\text{CeF}_4 \cdot 0.33\text{H}_2\text{O}$	-0.4	3.44	0.8	OH
	1.2	0.7	0.5	OH
	6.8	1.7	21.6	H <sub>2</sub> O
	6.8	5.1	77.0	H <sub>2</sub> O
	8.8	0.7	0.3	H <sub>2</sub> O

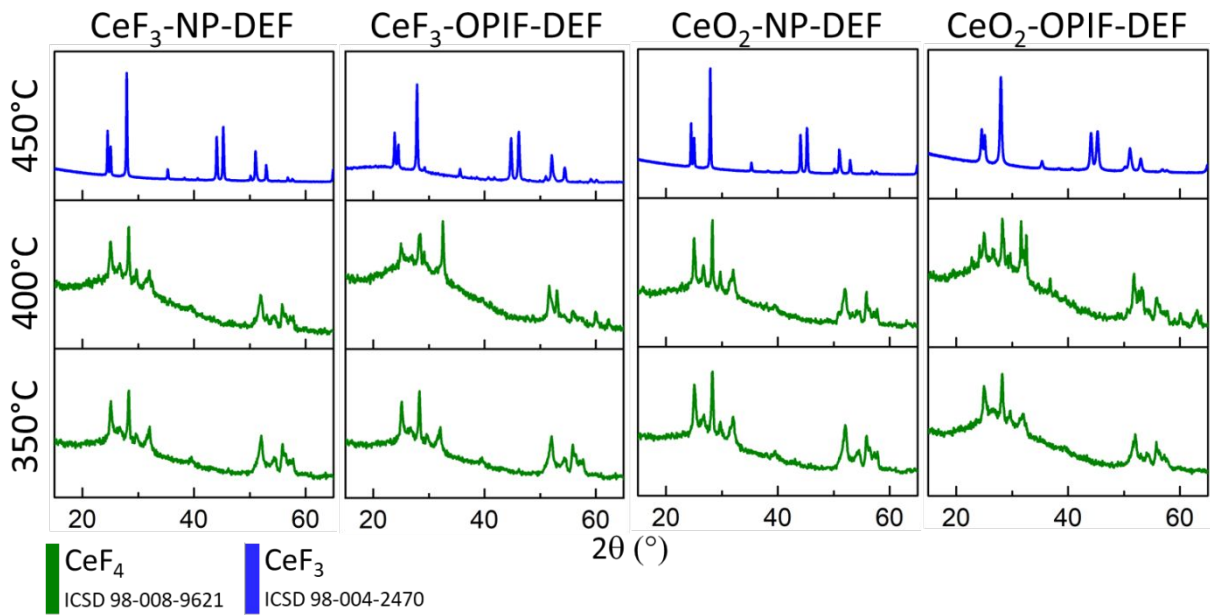


**Figure S17.** XRD patterns of CeF<sub>3</sub>-NP, CeF<sub>3</sub>-OPIF, CeO<sub>2</sub>-NP and CeO<sub>2</sub>-OPIF after defluorination under vacuum for 3h at different annealing temperatures.

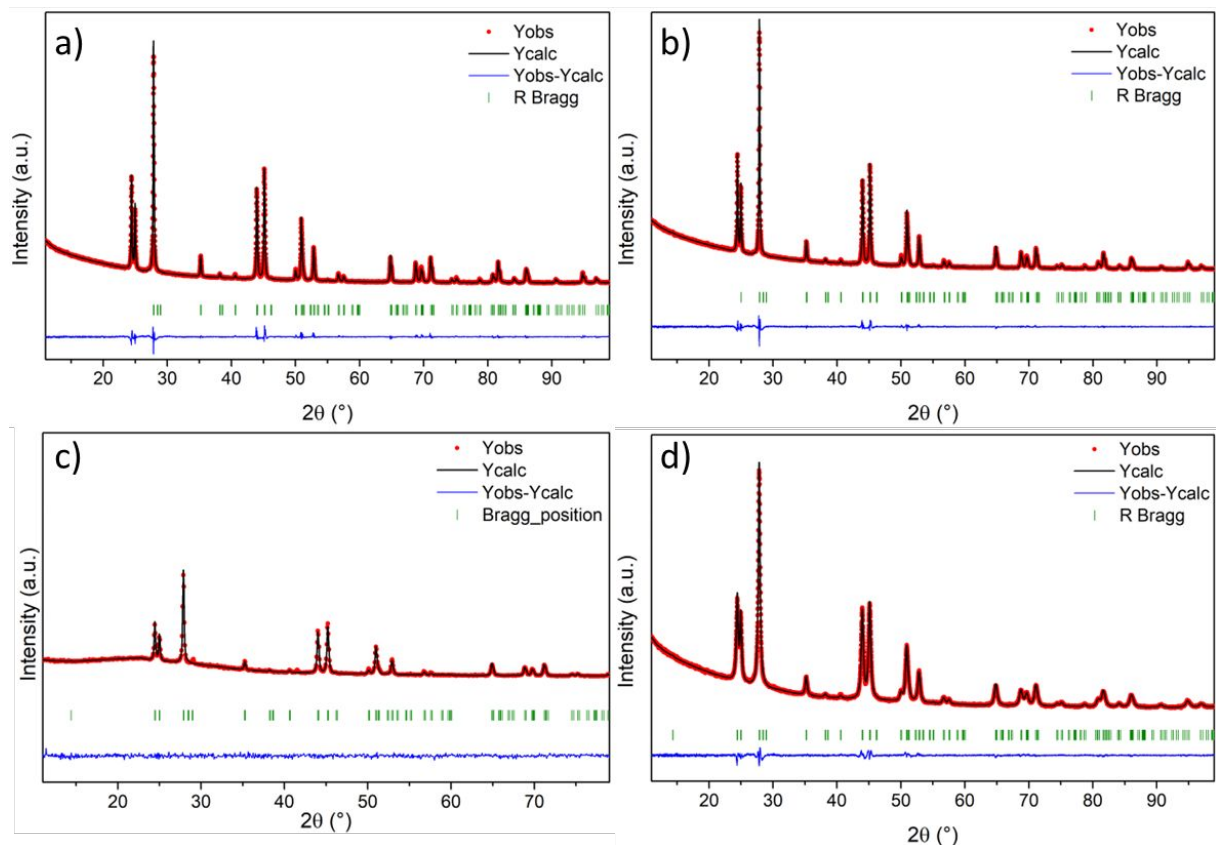


**Figure S18.** Rietveld refinement of the powder X-ray diffraction patterns of a) CeF<sub>3</sub>-NP-C1, b) CeO<sub>2</sub>-NP-C1, c) CeF<sub>3</sub>-OPIF-C1 and d) CeO<sub>2</sub>-OPIF-C1. Experimental in red, calculated in black and difference in blue. Vertical green lines mark the positions of CeF<sub>3</sub> reflections.

**Table S11.** Crystal data, data collection and structure refinement details of CeF<sub>3</sub>-NP-C1, CeF<sub>3</sub>-OPIF-C1, CeO<sub>2</sub>-NP-C1 and CeO<sub>2</sub>-OPIF-C1. CeF<sub>3</sub>: crystal system trigonal, space group: *P*3c1. Radiation type: CuK<sub>α</sub>, 2θ range (°): 6-100.

Sample	CeF <sub>3</sub> -NP-C1	CeF <sub>3</sub> -OPIF-C1	CeO <sub>2</sub> -NP-C1	CeO <sub>2</sub> -OPIF-C1
Phase	CeF <sub>3</sub>	CeF <sub>3</sub>	CeF <sub>3</sub>	CeF <sub>3</sub>
a (Å)	7.1297(8)	7.1238(2)	7.1287(2)	7.1323(9)
c (Å)	7.2892(1)	7.2807(3)	7.2877(1)	7.2929(3)
V (Å <sup>3</sup> )	320.895(2)	319.987(1)	320.734(2)	321.294(4)
Number of reflections	145	85	147	171
Number of parameters	40	41	43	43
R <sub>p</sub> /R <sub>wp</sub> (%)	10.8/9.56	15.6/12.5	10.6/8.71	8.06/7.04
R <sub>B</sub> /R <sub>f</sub> (%)	2.82/2.86	3.31/3.88	1.85/2.08	1.38/1.16
χ <sup>2</sup>	4.97	1.46	3.28	2.41
Coherent domain size <L> (Å)	651	528	887	264

**Table S12.** Mass losses under argon (TGA analysis) of the materials after one cycle.

	CeF <sub>3</sub> -NP-C1	CeF <sub>3</sub> -OPIF-C1	CeO <sub>2</sub> -NP-C1	CeO <sub>2</sub> -OPIF-C1
Mass loss (%)	9	9	11	12

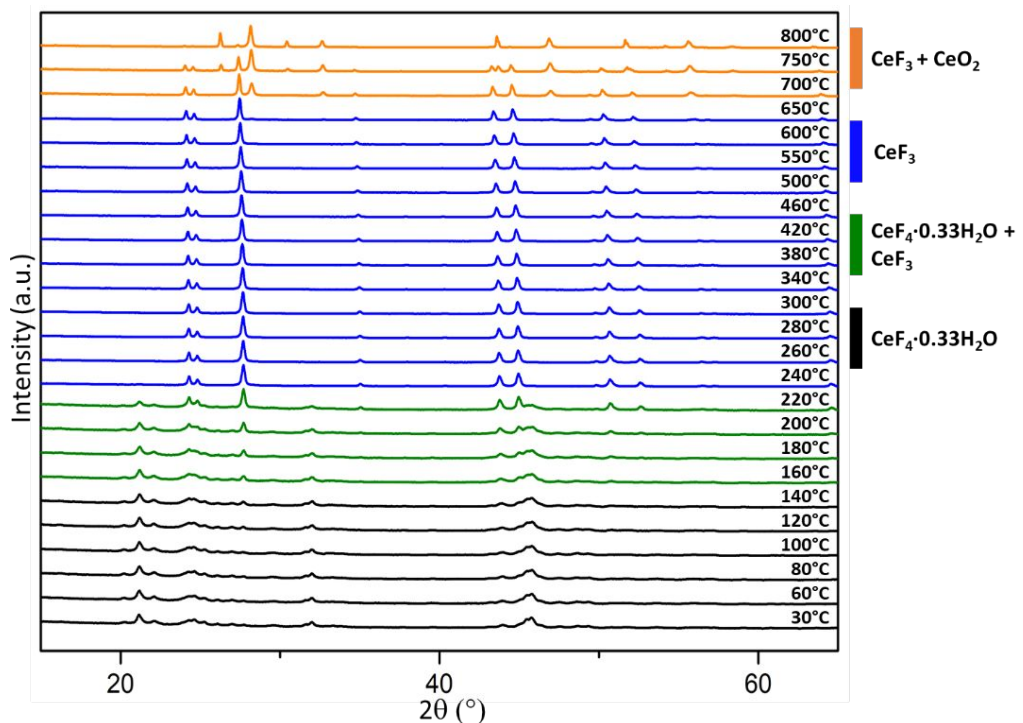


**Figure S19.** Variable temperature PXRD study of CeF<sub>4</sub>·0.33H<sub>2</sub>O under N<sub>2</sub>.

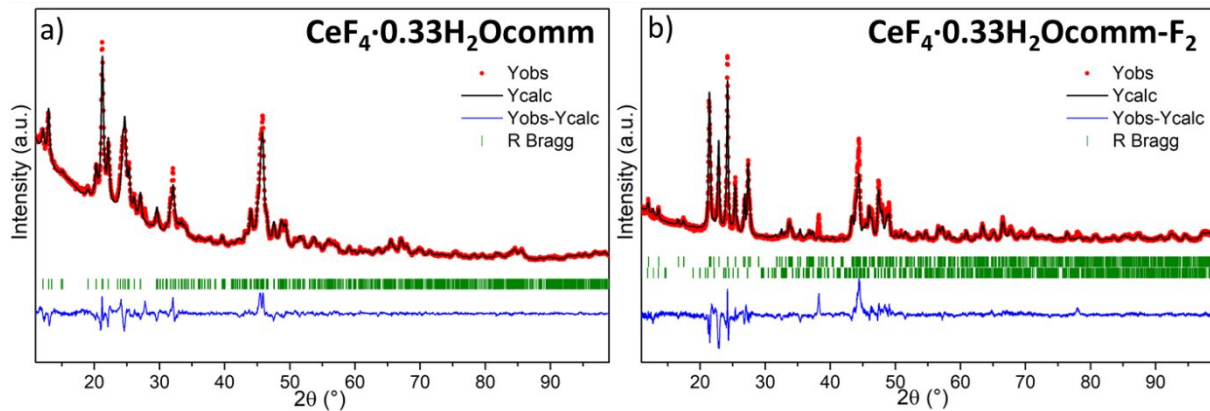


**Figure S20.** Rietveld refinement of the powder X-ray diffraction patterns of commercial  $\text{CeF}_4 \cdot 0.33\text{H}_2\text{O}$  a) as received and b) after one complete cycle (one defluorination and one fluorination). Experimental in red, calculated in black and difference in blue. Vertical green lines mark the positions of  $\text{CeF}_4$  and  $\text{CeF}_4 \cdot 0.33\text{H}_2\text{O}$  reflections.

**Table S13.** Crystal data, data collection and structure refinement details of commercial  $\text{CeF}_4 \cdot 0.33\text{H}_2\text{O}$  a) as received and b) after one complete cycle (one defluorination and one fluorination).  $\text{CeF}_4 \cdot 0.33\text{H}_2\text{O}$ : crystal system monoclinic, space group:  $I\bar{m}$ .  $\text{CeF}_4$ : crystal system monoclinic, space group:  $C2/c$ . Radiation type:  $\text{CuK}_{\alpha}$ ,  $2\theta$  range ( $^{\circ}$ ): 6-100.

Sample	$\text{CeF}_4 \cdot 0.33\text{H}_2\text{Ocomm}$	$\text{CeF}_4 \cdot 0.33\text{H}_2\text{Ocomm}-\text{F}_2$
Phase	$\text{CeF}_4 \cdot 0.33\text{H}_2\text{O}$	$\text{CeF}_4$
% mol	100	93
a (Å)	8.4390(6)	12.5971(0)
b (Å)	11.731(9)	10.6349(9)
c (Å)	9.3923(7)	8.2453(5)
$\beta$ ( $^{\circ}$ )	95.9611(43)	126.3198(7)
V (Å $^3$ )	924.822(118)	890.026(0)
Number of reflections	917	591
Number of parameters	20	17
$R_p/R_{wp}$ (%)	13.1/14.3	26.1/29.9
$R_B/R_f$ (%)	4.60/2.08	15.4/8.23
$\chi^2$	6.76	8.16
Coherent domain size $\langle L \rangle$ (Å)	157. <b>22</b>	316. <b>43</b>

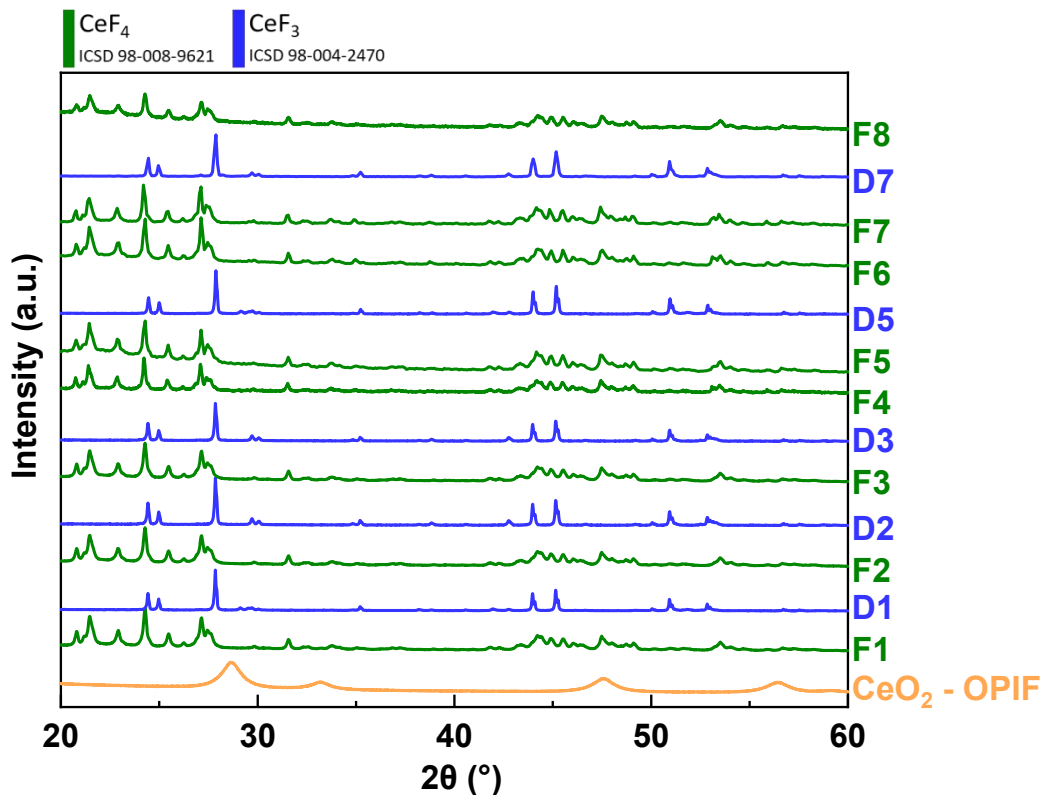


**Figure S21.** PXRD study of fluorination(F)/defluorination(D) cycles of  $\text{CeO}_2$ -OPIF.

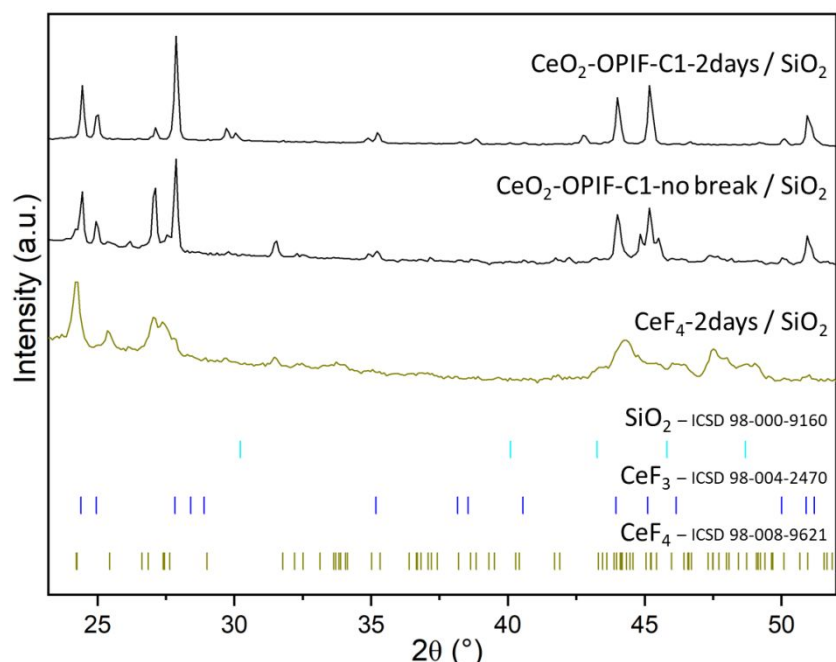


**Figure S22.** PXRD patterns recorded before ( $\text{CeF}_4$ -2days /  $\text{SiO}_2$ ) and after ( $\text{CeO}_2$ -OPIF-C1-2days /  $\text{SiO}_2$  and  $\text{CeO}_2$ -OPIF-C1-no break /  $\text{SiO}_2$ ) defluorination monited by gas-phase infrared under nitrogen ( $\text{N}_2$ ) with the presence of  $\text{SiO}_2$ .

**Table S14.** Theoretical volume occupied by CeF<sub>4</sub> materials (obtained with CeO<sub>2</sub> as starting material) in a 50 L cylinder, associated F mass and container-to-content mass ratio.

Sample	V <sub>cyl.</sub> (cm <sup>3</sup> )	V <sub>tot</sub> (cm <sup>3</sup> .g <sup>-1</sup> )	m(CeF <sub>4</sub> ) (g)	m(CeF <sub>4</sub> ) (kg)	m(F) (g)	m(F) (kg)	Mass ratio
CeF <sub>4</sub>	50000	0	119250	119.3	10494	10.5	5.2
CeF <sub>4</sub> -NP	50000	0.35	8940	89.4	787	7.9	6.8
CeF <sub>4</sub> -OPIF	50000	0.37	8627	86.3	759	7.6	7.1

The use of solid storage materials for the chemisorption of F<sub>2</sub> has the advantage of reducing the container-to-content mass ratio. As a reference, a 50 L cylinder has a mass of 54 kg for 2.2 kg of stored F<sub>2</sub>. The mass ratio of these metal cylinders is thus:  $\frac{m_{cyl.}}{m(F)} = \frac{54}{2.2} = 24.5$ .

**Table S14** summarizes the calculations of material masses for an absolute volume filling (if the porous volume is zero) and relative (taking into account intra- and intergranular porous volumes). CeF<sub>4</sub>-NP and CeF<sub>4</sub>-OPIF were not analyzed by nitrogen sorption to avoid any contamination of the apparatus due to the release of corrosive fluorine gas; the reported porous volumes (V<sub>tot</sub>) are those of MgF<sub>2</sub>-NP and MgF<sub>2</sub>-OPIF, whose particle and pore sizes are similar to those of cerium compounds (7 and 10 nm respectively, and D<sub>pores</sub> = 200 nm) as previously reported.<sup>1</sup> Note that the densities of CeF<sub>4</sub> and CeF<sub>3</sub> are 4.77 and 6.16 respectively, and that the mass loss associated with the release of half a mole of F<sub>2</sub> (CeF<sub>4</sub> ⇌ CeF<sub>3</sub> + ½ F<sub>2</sub>) is 8.8%. The masses of cerium tetrafluoride and associated fluorine are determined by the following relations:

$$m(CeF_4) = d(CeF_4) \times \frac{V_{cyl.}}{1 + d(CeF_4) \times V_{tot}}$$

$$m(F) = 0.088 \times m(CeF_4)$$

<sup>1</sup> Goharibajestani, Z.; Wang, Y.; Camus-Génot, V.; Arrii, S.; Comparot, J. D.; Polteau, B.; Lhoste, J.; Galven, C.; Gunes, V.; Hémon-Ribaud, A.; Pascual, S.; Body, M.; Legein, C.; Maisonneuve, V.; Brunet, S.; Guiet, A. MgF<sub>2</sub>-Based Organized Porous Inorganic Nanofluorides as Heterogeneous Catalysts for Fluorination of 2-Chloropyridine. *ACS Appl. Nano Mater.* **2021**, *4*, 10601–10612. <https://doi.org/10.1021/acsanm.1c01768>.